Journal of Rock Mechanics and Geotechnical Engineering 11 (2019) 61–71

Contents lists available at ScienceDirect

Journal of Rock Mechanics and Geotechnical Engineering

journal homepage: www.rockgeotech.org

Full Length Article

Strip loading test theory and equipment development

Jiliang Li

Department of Mechanical and Civil Engineering, Purdue University Northwest, Hammond and Westville, Indiana, USA

ARTICLE INFO

Article history:
Received 12 December 2017
Received in revised form
26 June 2018
Accepted 2 July 2018
Available online 17 November 2018

Keywords:
Strip loading test
Soil properties
Strength parameters
Cohesion
Internal friction angle

ABSTRACT

One of the important issues for geotechnical engineers is the characterization of soil properties such as cohesion and internal friction angle by means of soil testing. A new experimental method of soil characterization based on the surface displacement of strip loaded soils is proposed. The theory to relate the soil deformation/displacement to soil strength properties is presented and compared with a series of conventional soil characterization techniques with direct shear tests. The proposed/developed strip loading tests provide reasonably accurate results compared with traditional direct shear tests. The new strip loading physical simulation and testing devices are helpful for understanding soil strength concepts and also provide an effective bridge connecting with engineering mechanics and foundation engineering courses instructions wherein derivation of bearing capacity theory equations is based on the same Mohr-Coulomb soil strength parameters. The advantages, limitations, and use of the strip loading modeling/testing technique in engineering education and further more in depth researches are discussed in the concluding remarks part.

1. Introduction

Soil strength is the capacity of a soil to withstand induced stresses within a soil body without experiencing failures such as rupture, fragmentation, and flow (Scott, 1963). Depending on different paths and modes of loading, soils exhibit different capacities to resist failure and thus different strength values. In geotechnical engineering, most of the normal stresses induced within the soils are compressive. However, shear stresses exist in certain directions within the soil resulting in the dominant shear failure mode.

Numerous researchers and engineers have studied various kinds of geotechnical problems related to soil strength properties. For example, Gadry (1746) observed the existence of slip planes in a soil at failure. Darwin (1883) presented test data on sand and indicated how the arrangement of grains (and hence the relative density) affects strength. Coulomb (1776) reported that the strength function consists of two parameters: cohesion, c, and friction resistance due to internal friction angle, ϕ. Mohr (1900) presented the theory that rupture in materials is caused by a critical combination of normal and shear stresses at failure. Detailed procedures of conducting triaxial compression and tension tests for strength properties were suggested by Bishop and Henkel (1962), Bishop and Wesley (1975). Rowe (1962) related the stress, dilatancy and internal friction angle to the soil sliding angle and the effect of interlocking within the soil. Later, many more modern soil characterization models (Whittle, 1991; Jefferies, 1993; Cui et al., 2000; Zhang and Ikariya, 2011) were developed with modifications and improvements to the Cam Clay type models (Chen and Baladi, 1985) and Nor Sand model has also stemmed from critical state soil mechanics. Demonstration models for undergraduate teaching geotechnics have been introduced and highlighted by Bucher (1986). Physical models have served important functions in engineering research, practice, and education for hundreds of years (Ferguson, 1992). Guo et al. (2002) edited a special proceeding of physical modeling in geotechnics due to their increasing importance in geotechnical engineering education, research and practice. Wood (2004) published his well-known geotechnical modeling textbook. Wartman (2006) also emphasized the geotechnical physical modeling for education via the learning theory approach. There are many other different evaluation methods developed for in situ soil shear strength, such as standard penetration test (SPT), cone penetration test (CPT), pressuremeter test (PMT), dilatometer test (DMT), plate load test (PLT), and improved direct shear and triaxial shear testing devices. However, there appears to be no immediate connection with shallow foundation failure mechanism associated soil strength testing device development reported and hence there is a need to develop such an intuitive, simple and yet effective soil strength strip loading test device and teaching aids.

E-mail address: li1919@purdue.edu.

Peer review under responsibility of Institute of Rock and Soil Mechanics, Chinese Academy of Sciences.

https://doi.org/10.1016/j.jrmge.2018.07.005

Soil shear strength properties must be correctly and approximately determined and evaluated for any approximately adequate analysis and design of any structures built on or within the earth. The traditional soil testing methods, such as the triaxial and direct shear tests, are used for determining soil strength parameters. However, they are either very expensive or time-consuming to perform due to the requirement of complicated testing procedures or not fully reliable due to the lack of qualified and competent testing staff. Also, these methods are mostly only used in the laboratory which however may not be that often applied for in situ field testing.

A laboratory-scale soil strength physical modeling/testing device based on strip footing is developed for enhancing the educational research purposes of geotechnical and foundation engineering. This strip loading test method provides students with intuitive understanding of soil shear strength parameters. It can be used as an effective instruction device connecting undergraduate courses instructions from a basic mechanics course of statics to senior and graduate level course of foundation engineering. Additional research to refine the developed strip loading testing theory and device could also be utilized for calibration research purpose of soil plasticity constitutive model as well. The improved in situ strip loading test may also be used for field testing with further research and improvement.

2. The strip loading test method

Soil models require input from basic material property tests of soils. There are several different traditional laboratory testing methods for characterizing soil strength properties, including the direct shear test and triaxial shear test (Bishop and Henkel, 1962; Bishop and Wesley, 1975). Most of the existing methods essentially use a small soil specimen.

As an alternative, a new method was introduced and developed to determine the soil strength properties (Li, 2005). The testing apparatus includes devices for strip loading and for non-contact measurement of the displacement on granular surfaces. Park and Li (2004) reported the technique and the system in their study of subsidence simulations. The main aim of this paper is to evaluate the soil strength properties by measuring the surface deformation range induced by a strip footing load, in conjunction with force/stress equilibrium and limit moment analysis (Li, 2005; Li et al., 2007). Based on the developed equipment, Kim (2008) further refined and improved the soil shear strength testing device. Using a laboratory-scale subsidence modeling/testing device, Li and Zhai (2015) explored and reported the soil shear strength estimation with subsidence modeling device.

The newly developed testing method uses a sand box (12.5 in $\times$ 10 in $\times$ 6 in or 317 mm $\times$ 254 mm $\times$ 152 mm) that holds a relatively large size of soil specimen on which vertical strip loading is applied. Thus, this new method can work on a relatively larger scale compared with traditional laboratory testing methods. The soil strength properties determined from the proposed method are the average of the mobilized strength of all the soils below the strip footing. This testing method was inspired by the analyses of the general shear failure phenomenon for the strip foundation. The basic structure of the formulae used for calculations of bearing capacity has a similar form as the one developed by Terzaghi (1943) and the actual failure mechanism diagram adopted follows that of De Beer and Vesic (1958) and Vesic (1973).

2.1. Theoretical analysis of failure by strip loading

Besides excessive settlement failure in soil foundation, bearing capacity is another important parameter for shallow foundation design (Taylor, 1948; Vesic, 1973; Leshchinsky and Marcozzi, 1990; Das, 1987, 2018; Holtz et al., 2011). When the magnitude of the induced shear stresses exceeds that of the shear strength of the soil, general shear failure may occur. This type of general shear failure often occurs suddenly along the surfaces of dense sand (or stiff clayey soil) extending to a great depth than foundation width $B = 2X$ (X is the half of strip footing width), as illustrated in Fig. 1, and is often observed as a bulge on the ground surface adjacent to the foundation. When the load Q_u on the foundation is gradually increased, the load per unit area $q_u = Q_u/A$ (A is the area of foundation) will increase and the foundation will undergo sudden shear failure when q_u becomes equal to peak stress q_u corresponding to foundation settlement $s = s_u$. The soil supporting the strip footing in Fig. 1 will suddenly undergo general shear failure. A schematic diagram of general shear failure surface in the soil is shown in Fig. 1a with a corresponding load settlement curve, as shown in Fig. 1b, wherein a peak value q_u is clearly observed.

The soil is assumed to fail along the curves shown in Fig. 1a (De Beer and Vesic, 1958), based on the improvement to Terzaghi (1943). The strip footing of width B is buried under the soil with embedment depth, D_f. The unit weight of soil is γ. The soil general shear failure mechanism below the strip footing theoretically has three distinct zones (Terzaghi, 1943; Terzaghi et al., 1996). Zone I is the elastic compression active pressure zone (Prandtl, 1921), also known as the wedge zone, which is the soil part immediately beneath the strip footing. Zone I is considered to remain intact and moves downward when the strip footing load is applied on the foundation soil. Zone II is the transition zone, or the radial shear zone, which extends from each side of the wedge. The shape of the shear planes is assumed to be part of a logarithmic spiral because it preserves compatibility caused by dilatancy (Taylor, 1948; Bolton, 1986). Zone III is the passive pressure zone (Prandtl, 1921), also known as the linear shear zone, where soil shears along planar surfaces.

The prime objective of the article is to enhance education of soil strength theory in geotechnical engineering and strip footing in foundation engineering based on the study reported by Li (2005) and Kim (2008). Therefore, at this stage, only the conventionally accepted Mohr-Coulomb theory is adopted. Though the latest development of soil strength dilatancy (Taylor, 1948; Bolton, 1986) may be resolved to better help accurately evaluate the soil dilatancy angle and critical state friction angle, the recommended framework was not attempted at this stage. The author hopes to delve into that investigation in another separate article.

2.2. Limit equilibrium analysis

Fig. 2 shows one of the most widely used limit equilibrium analyses for computing bearing capacity of soils (Terzaghi, 1943). This method of limit equilibrium analysis is based on the following assumptions:

(1) The width B is larger than the surcharge depth D_f, as defined in Fig. 1;
(2) The foundation is rough and rigid;
(3) The soil below is a homogeneous semi-infinite mass;
(4) The Mohr-Coulomb strength of the dry sandy soil, with pore water pressure u being zero, is assumed to be in the form of $\tau = c + \sigma\tan\phi$, where σ is the normal stress;
(5) The general shear mode of failure governs;
(6) The soil consolidation is neglected (i.e. settlement is assumed only by the shearing and lateral movement of the soil);
(7) The soil between the ground surface and the depth D_f has no shear strength, and serves only as a surcharge load; and
(8) The vertically applied strip load is compressive and to the centroid of the strip and with no applied moment.

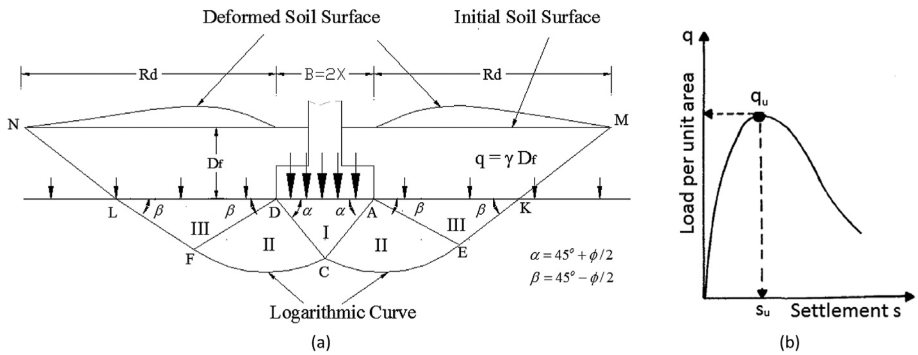

Fig. 1. Bearing capacity failure in soil under a strip foundation.

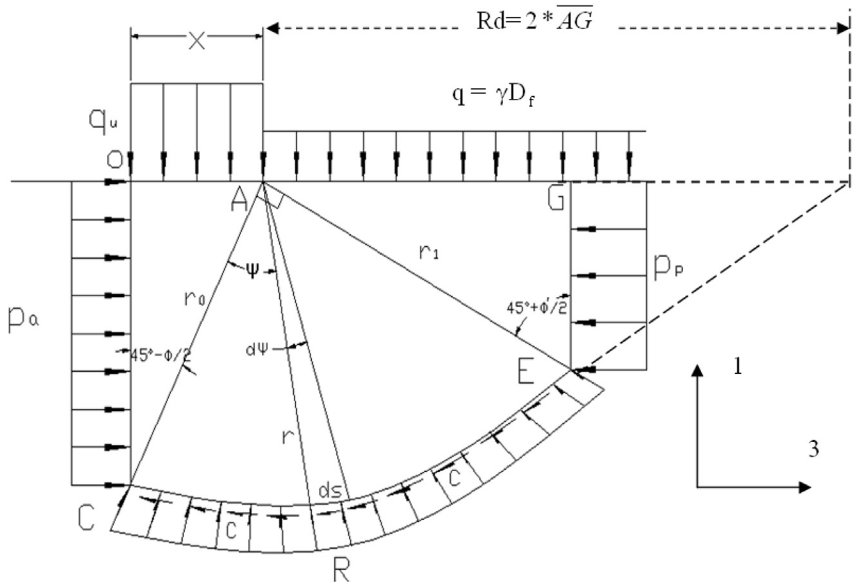

Fig. 2. Simple limit equilibrium analysis.

Based on the above assumptions and the limit equilibrium of force and moment analyses, the strip footing failure analysis is carried out, and a new method of measuring the Mohr-Coulomb soil material parameters, including the cohesion c and the internal friction angle ϕ, is established. At the initial stage of the research project, the analytical development was performed. According to the general failure of strip footing illustrated in Fig. 1, the soil failure below the strip footing obeys the limit equilibrium condition (Das, 1987, 2008, 2016, 2018), for which a force diagram can be drawn, as shown in Fig. 2.

In Fig. 2, ψ is the angle between current arbitrary log spiral radius r and AC, r_0 is the initial length radius of the logarithmic spiral (AC), r_1 is the final length radius of logarithmic spiral (AE), p_a is the Rankine active pressure in Zone I, p_p is the Rankine passive pressure in Zone III, $q = \gamma D_f$ is the overburden stress induced by surcharge thickness D_f, and ϕ' stands for the effective internal friction angle or just internal friction angle ϕ when the dry soil is tested.

The line segment $\overline{OA}$ is the area where ultimate bearing capacity q_u is applied, $\overline{AG}$ is the area where the effective stress $q = \gamma D_f$ is applied at the level of the bottom of the foundation, and $\overline{OC}$ is the area where Rankine active pressure p_a is applied. In the Rankine active pressure failure Zone I (Das, 1987, 2008, 2018), we have

$$\sigma_3 = \sigma_1 \tan^2\left(45^\circ - \frac{\phi}{2}\right) - 2c\tan\left(45^\circ - \frac{\phi}{2}\right) \tag{1}$$

where σ_3 is the minor principal stress, also known as horizontal Rankine active principal stress p_a; and σ_1 is the major principal stress, equal to vertical ultimate bearing capacity pressure q_u. $\overline{GE}$ is the area where Rankine passive pressure p_p is applied. In the Rankine passive pressure failure Zone III (Das, 1987, 2018), we have

$$\sigma_1 = \sigma_3 \tan^2\left(45^\circ + \frac{\phi}{2}\right) + 2c\tan\left(45^\circ + \frac{\phi}{2}\right) \tag{2}$$

where σ_1 is equal to the horizontal passive principal stress σ_p or horizontal stress σ_h, and σ_3 is equal to the vertical surcharge load q. Hence, from Zone I to Zone III, there is a major and minor principal stresses rotation. The geometric relationships of the strip foundation and failed soil are written as follows:

$$\left.\begin{array}{l} \overline{OA} = X,\ \overline{OC} = \dfrac{X}{\tan\left(45^\circ - \dfrac{\phi}{2}\right)},\ \overline{AC} = r_0 = \dfrac{X}{\sin\left(45^\circ - \dfrac{\phi}{2}\right)} \\ \overline{GE} = r_1\cos\left(45^\circ + \dfrac{\phi}{2}\right),\ \overline{AG} = r_1\sin\left(45^\circ + \dfrac{\phi}{2}\right) \\ r = r_0 e^{\psi\tan\phi},\ r_1 = r_0 e^{\pi\tan\phi/2} \end{array}\right\} \tag{3}$$

Considering the moment equilibrium of the body about point A (Prandtl, 1921; Terzaghi, 1943; Das, 1987, 2008, 2018; Li, 2005;

Terzaghi et al., 1996; Chen and Zhou, 2008; Hibbeler, 2016; Beer et al., 2019), we have

$$\sum M_A = 0 \tag{4}$$

$$q_u \frac{X^2}{2} + p_a \frac{\overline{OC}^2}{2} = q \frac{\overline{AG}^2}{2} + p_p \frac{\overline{GE}^2}{2} + M_R + M_c \tag{5}$$

where M_R is the moment due to resistant force R, and M_c is the moment due to cohesion about point A. Since the support resistance force R is all assumed to go through the logarithm curve center A, we have $M_R = 0$.

In Fig. 3, the angle between the direction of resultant force R and the normal direction n to the failure surface is the same as the internal friction angle ϕ, according to Das (1987).

From the mathematical analysis, the integration of the moment of cohesion, M_c, along the arc length ds can be written as follows:

$$M_c = \int cr \cos \phi \mathrm{d}s \tag{6}$$

where ds is the arc length, which can be approximated as $\mathrm{d}s = r\mathrm{d}\psi/\cos\phi$ in the approximated triangle ΔKLM. Hence, Eq. (6) can be rewritten as

$$M_c = \int cr^2 \mathrm{d}\psi \tag{7}$$

With Eq. (7) and at an interval [0, π/2], we have

$$M_c = \int_0^{\pi/2} cr^2 \mathrm{d}\psi = cr_0^2 \int_0^{\pi/2} \left(\mathrm{e}^{\psi \tan \phi}\right)^2 \mathrm{d}\psi$$
$$= \frac{cr_0^2}{2\tan\phi}\left(\mathrm{e}^{\pi \tan \phi} - 1\right) \tag{8}$$

If the given values of p_a, p_p, $M_R = 0$, M_c (Eq. (8)) and the various lengths of boundaries are substituted into Eq. (5), the following relationship can be obtained (Li, 2005):

$$\frac{q_u X^2}{2} + \left[q_u \tan^2\left(45^\circ - \frac{\phi}{2}\right) - 2c\tan\left(45^\circ - \frac{\phi}{2}\right)\right] \frac{\left[\frac{X}{\tan\left(45^\circ - \frac{\phi}{2}\right)}\right]^2}{2}$$
$$= q\frac{\left[r_0 \mathrm{e}^{\pi \tan(\phi/2)} \sin\left(45^\circ + \frac{\phi}{2}\right)\right]}{2} + \left[q\tan^2\left(45^\circ + \frac{\phi}{2}\right) + 2c\tan\left(45^\circ + \frac{\phi}{2}\right)\right] \frac{\left[r_0 \mathrm{e}^{\pi \tan(\phi/2)} \cos\left(45^\circ + \frac{\phi}{2}\right)\right]^2}{2}$$
$$+ \frac{cr_0^2}{2\tan\phi}\left(\mathrm{e}^{\pi \tan \phi} - 1\right) \tag{9}$$

where

$$r_0 = \overline{AC} = \frac{X}{\sin\left(45^\circ - \frac{\phi}{2}\right)} \tag{10}$$

The internal friction angle ϕ can be determined from the newly developed soil surface deformation measurement device. Derivation of Eq. (9) is needed and necessary as it can be seen that evaluation of the cohesion c is made possible by measurement of both the failure load q_u and soil internal friction angle ϕ first.

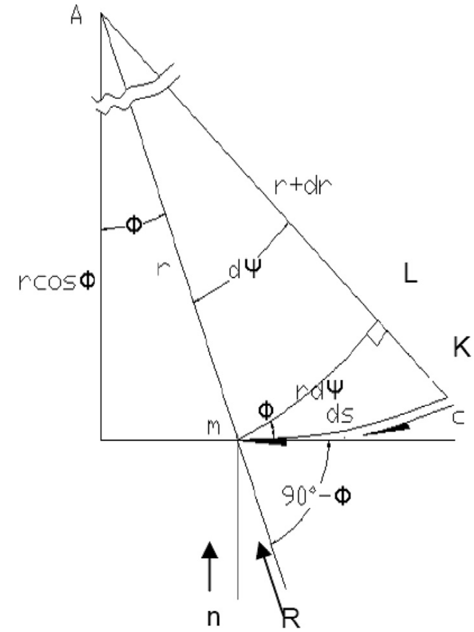

Fig. 3. Expanded log spiral curve section in Fig. 2.

2.3. Determination of soil strength properties

With $\overline{AG} = r_1 \sin(45^\circ + \phi/2)$, we can obtain the internal friction angle as (Li, 2005):

$$\phi = 2\left[\sin^{-1}\left(\frac{\overline{AG}}{r_1}\right) - 45^\circ\right] \tag{11}$$

where $\overline{AG} = R_d/2$. The next step is to define the surface deformation range $R_d = 2\overline{AG}$. Physically, it is half of the width of the surface deformation area minus half of the strip width, X.

If $R_d/2$ is inserted in place of $\overline{AG}$ into Eq. (11), it becomes (Li, 2005):

$$\phi = 2\left[\sin^{-1}\left(\frac{R_d}{2r_1}\right) - 45^\circ\right] \tag{12}$$

Also, substituting $r_1 = r_0 \mathrm{e}^{\pi \tan \phi/2}$ into Eq. (12) again, we have the following equation (Li, 2005):

$$\phi = 2\left\{\sin^{-1}\left[\frac{R_d}{2r_0 \mathrm{e}^{\pi \tan(\phi/2)}}\right] - 45^\circ\right\} \tag{13}$$

By inserting Eq. (10) into Eq. (13), following equations are derived (Li, 2005; Li et al., 2007):

$$\phi = 2\left\{\sin^{-1}\left[\frac{\sin\left(45^\circ - \frac{\phi}{2}\right) R_d}{2X \mathrm{e}^{\pi \tan(\phi/2)}}\right] - 45^\circ\right\} \tag{14}$$

where

$$R_d = 2X\sqrt{\frac{1+\sin\phi}{1-\sin\phi}} \mathrm{e}^{\pi \tan(\phi/2)} = 2X\tan\left(\frac{\pi}{4} + \frac{\phi}{2}\right)\mathrm{e}^{\pi \tan(\phi/2)} \tag{15}$$

Thus, the equation for determining the internal friction angle is derived, by which the internal friction angle ϕ can be determined from the newly developed soil surface deformation measurement device. R_d can be obtained from the soil surface deformation measurement device using laser scanning and potentiometers. In the following strip loading tests, Eq. (15) is used to estimate R_d because of strip loading on the surface with the surcharge depth D_f being equal to zero. Eq. (15) illustrates that surface deformation range is scale-dependent on the full strip foundation width, $2X$, and is also a nonlinear function of soil internal friction angle ϕ. For the strip loading on fully saturated clay soil wherein the soil internal friction angle ϕ is close to zero and thus could be assumed 0°, then Eq. (15) could be reduced to $R_d = 2X$ which indicates that the theoretical surface deformation range will be about the width of strip foundation. This has also been theoretically approved and reported by Budhu (2011) in his collapse load analysis using limit equilibrium analysis. Therefore, the derived surface deformation range equation R_d can be considered as a generalized special case as reported in Budhu (2011).

It is easy to see that Eqs. (14) and (15) are nonlinear. To solve this problem, a numerical program was developed according to Eq. (15). Fig. 4 is used to illustrate how the internal friction angle can be determined by measuring the soil surface deformation range from a test.

Once the friction angle is determined, as shown in Fig. 4, the value is used to evaluate Eq. (9) to determine the cohesion c. The soil cohesion is a function of soil internal friction angle ϕ, the ultimate bearing capacity q_u, and the surcharge load q, as illustrated in Eq. (16) and derived and discussed in Li (2005):

$$c = \frac{q_u(1 - \sin \phi) - q e^{\pi \tan \phi}(1 + \sin \phi)}{\cos \phi + e^{\pi \tan \phi} \cos \phi + (e^{\pi \tan \phi} - 1)\cot \phi} \tag{16}$$

The physical meaning behind Eq. (16) shows that the apparent soil strength parameter, cohesion c, is also related to the soil internal friction angle ϕ, surcharge load q at the strip buried depth D_f and most importantly the ultimate failure load pressure q_u. Eq. (16) is applicable as a generalized shear testing including the special triaxal shear test wherein the confining pressure is zero, also known as unconfined compression load test on a fully saturated clay soil. Likewise, for the fully saturated clay, it is often assumed that soil internal friction angle ϕ is close to and equal to 0°. If the strip plate is laid on the top of soil surface, then $q = 0$ kPa, and substituting $\phi = 0°$ into Eq. (16) will lead the equation to the reduced form of $c = 0.5q_u$ (kPa) which is how the soil strength parameter c (also known as undrained shear strength C_u or S_u) often estimated routinely by geotechnical engineers in the industry. For example, the often performed routine tests such as unconfined compression test and hand-held pocket penetration test are special cases of the derived equation. Therefore, we can also draw a conclusion that Eq. (16) can be considered as a generalized form of unconfined compression tests applicable to cohesive and frictional soil including both sandy and clayey soils exhibiting both soil frictional strength due to the soil internal friction angle ϕ and cohesive strength due to cohesion c. For testing sandy soil, if unconfined compression test is not possible, a corresponding test applicable to cohesive soils' unconfined compression test could thus be replaced by this developed strip loading test for quick measurement and estimation of soil strength parameters.

Therefore, the shear strength properties can be theoretically determined based on the limit equilibrium analysis. To obtain the cohesion c, a program was written to solve the soil cohesion that corresponds to different ultimate bearing capacities q_u, surcharges q, and internal friction angles ϕ. Fig. 5 shows how the cohesion can be determined with the failure load and internal friction angle determined. For example, if the soil below the strip fails at 17 kPa, and the internal friction angle of the soil is found to be 27° from Fig. 4, then the cohesion c can be estimated/determined from Fig. 5 to be approximately 0.7 kPa.

Using Eqs. (14) and (16), the shear strength properties can be determined. As a newly developed testing technique, further calibration and correlation processes have to be performed in order to generate more reasonable data. The following sections introduce the development of the soil surface measurement device and some typical analysis of the specimens of scanned soil surface deformation after strip loading to general shear failure.

3. Development of soil surface deformation measurement technique

As a surface deformation measurement technique, the laser optical triangulation distance measurement (OTDM) technique was employed. OTDM is an accurate and effective tool for measuring displacement even on a granular material surface caused by vertical loading. In an OTDM, a laser diode in the sensor projects a visible light spot onto the target surface. The spot is imaged on a charge coupled device by a receiver lens. The measured values are processed digitally and output as an analog current signal for vertical displacement. The resolution can reach an accuracy of 1 μm for a transducer transmitting to a smooth steel surface. The maximum range of measurement for the sensor used in this experiment was from 45 mm (1.8 in) to 95 mm (3.7 in). Its linearity of full-scale output was within ±0.2%.

Figs. 6 and 7 show the design of the surface displacement measurement system. A draw wire potential sensor (DWPS) is used to measure horizontal position, and an OTDM sensor is used to measure vertical surface deformation. An OTDM translator, which is attached to the beam of the overhang bar, moves horizontally to scan the soil surface deformation. Under the overhang bar, the sand box model is placed. This system was tested earlier with a subsidence simulation model composed of a sand box and a cavity generating device located on the bottom of the box. The physical modeling of subsidence monitoring on the sand surface was successfully performed (Park and Li, 2004) and later utilized in estimating soil shear strength parameter (Li and Zhai, 2015) via subsidence modeling test.

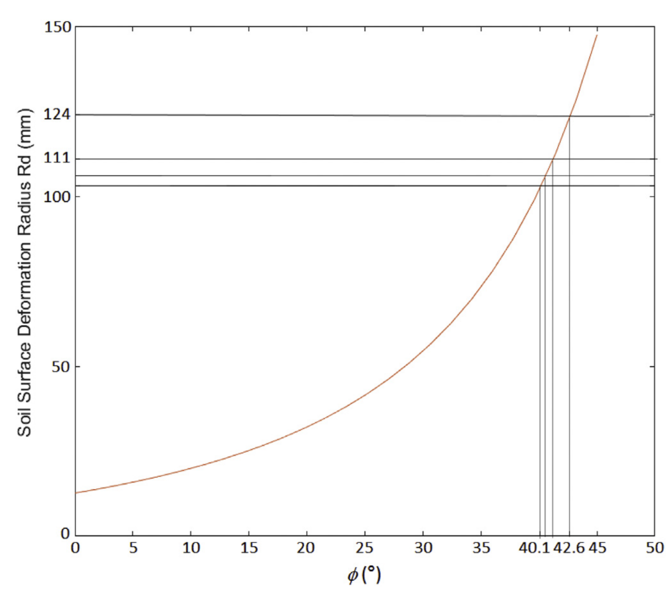

Fig. 4. Vertical surface deformation range vs. internal friction angle.

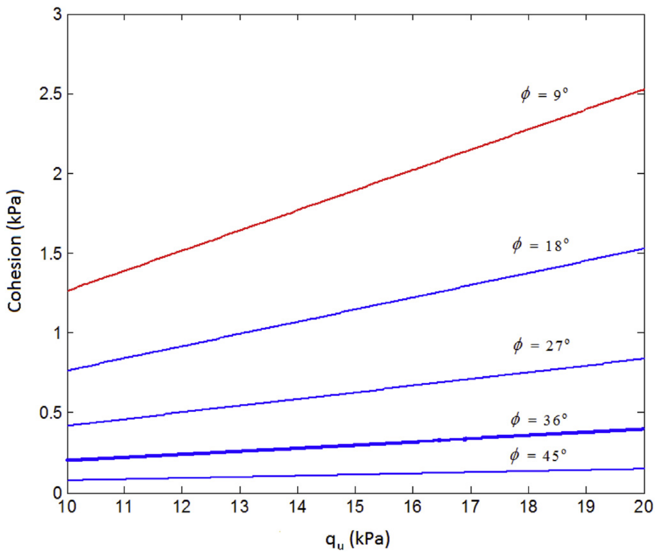

Fig. 5. Soil cohesion with respect to different q_u and ϕ values.

4. Strip loading test apparatus

A rectangular sand box frame (12.5 in × 10 in × 6 in or 317 mm × 254 mm × 152 mm) was built with a metal plate to hold soil specimens (Fig. 8). A frame is attached on two sides of the box. On the top of the frame, a mini-hydraulic jack is attached, and a strip loading rectangular plate is attached. The jack is carefully extended to load the plate observing the rate of the vertical displacement. When the rate starts to increase showing the start of general shear failure, loading is stopped immediately and the frame is removed. The surface's elevation is scanned again using the OTDM to determine the surface displacement profile.

A dry soil specimen as well as mixed soil specimens and natural specimens has been used for the strip loading tests (Li, 2005; Kim, 2008). For example, from a series of sieve analysis, the particle size distribution was determined, as shown in Fig. 9 (Li, 2005). The soil was mostly sand with some amount of fines.

5. Results of strip loading test

Fig. 10a shows a typical test result of a 1.27 cm (0.5 in) wide, 12.7 cm (5 in) long strip loading. As can be seen, the bulging areas on both sides of the loading strip are nearly symmetrical.

It is very important to determine the accurate width of the bulging area R_d, since it is directly related to the internal friction angle ϕ. Fig. 11 shows the curve fitting of the left wing of bulging on the strip loading test data shown in Fig. 10a. By analyzing the 1st and 2nd derivatives of the deformation profiles and the integral of the area of the bulging deformation profile, data necessary to determine R_d can be obtained. After finding R_d, ϕ is calculated according to Eq. (14) and c is calculated according to Eq. (16).

6. Discussion and analysis

Five tests were performed by Li (2005) using two strip sizes: 12.7 mm × 127 mm and 19.05 mm × 127 mm. As shown in Table 1, for loose sandy soil specimens prepared without compaction, the average internal friction angle is 41.2° and the average cohesion is 2.491 kPa for the 12.7 mm wide strip, and 38° and 2.637 kPa for the 19.05 mm wide strip, respectively. Plugging the average internal friction angle of 41.2° measured by strip loading test into Eq. (15) also verifies that the estimated soil internal friction angle from the 12.7 mm wide strip loading tests leads to theoretically approximately the same deformation range of 110 mm.

Direct shear test was conducted on the same soil specimen. The average internal friction angle measured is 36° and the average cohesion is 7 kPa for loose sandy soil specimen, as shown in Table 2. Compared with traditional direct shear test, the newly developed strip loading test has a relatively lower estimate of cohesion of 2.753 kPa, but a larger estimate of internal friction angle.

Based on geomaterial characterization equipment developed by Li (2005), Kim (2008) carried out additional six more strip loading tests and refined the developed strip loading test results. Table 1 also shows that the average internal friction angle of the mixed soil specimens tested with the developed strip loading test device has a range of 28.68°–38.1° and the cohesion of 2.637–7.862 kPa. Direct shear tests reported by Kim (2008) in Table 3 show an average internal friction angle of 31.63° and average cohesion of 16.7 kPa for the mixed soil specimens.

The proposed and developed strip loading tests were further refined and additional six field and mixed soil specimens were tested by Kim (2008) using two different strip sizes: 19.05 mm × 127 mm and 25.4 mm × 127 mm. As shown in Table 1, the average internal friction angle is 31.84° and the average cohesion is 2.64 kPa for the mixed soil specimens from the 19.05 mm wide strip loading test, and 32.51° and 7.862 kPa for the 25.4 mm wide strip loading test, respectively.

Direct shear test was conducted by Kim (2008) on the field soil specimen and mixed sandy, silt and clay soil specimen. The

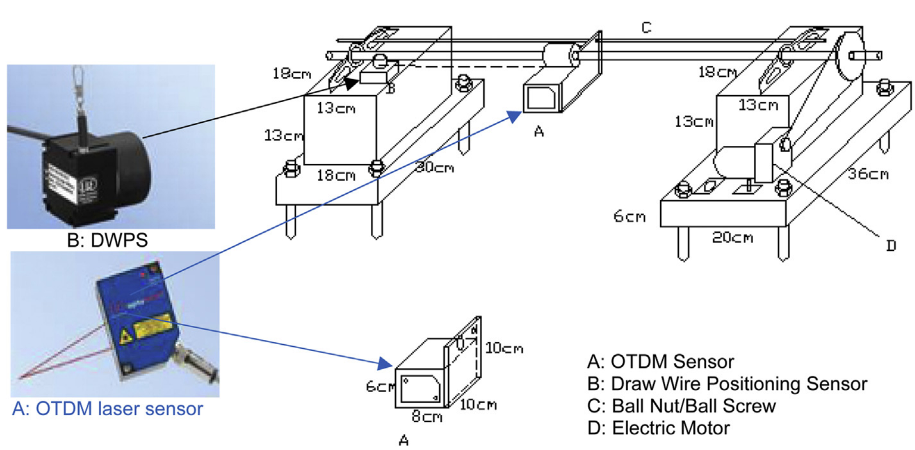

Fig. 6. Schematic diagram of surface displacement measurement system.

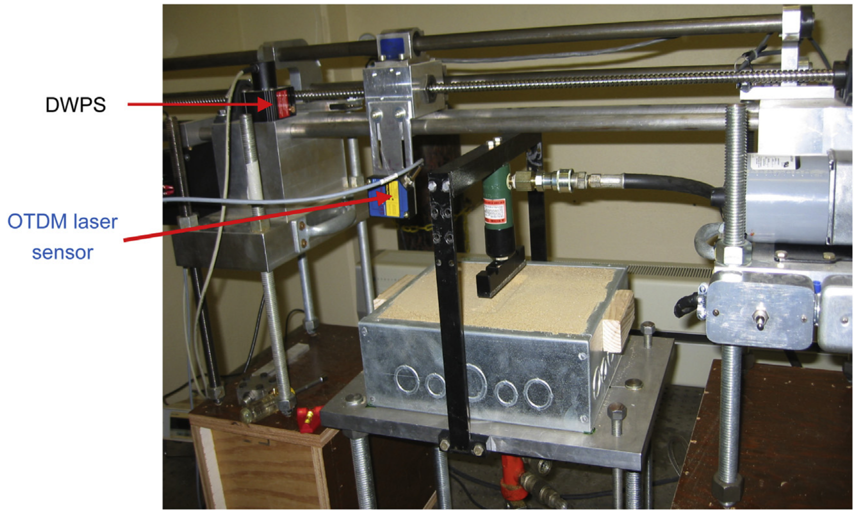

Fig. 7. Photo of surface displacement measurement system.

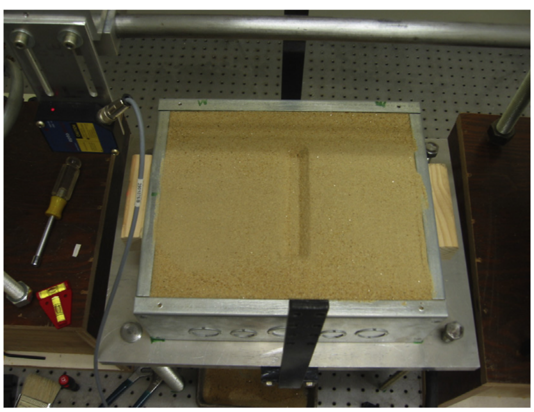

Fig. 8. Strip foot loading model (top view).

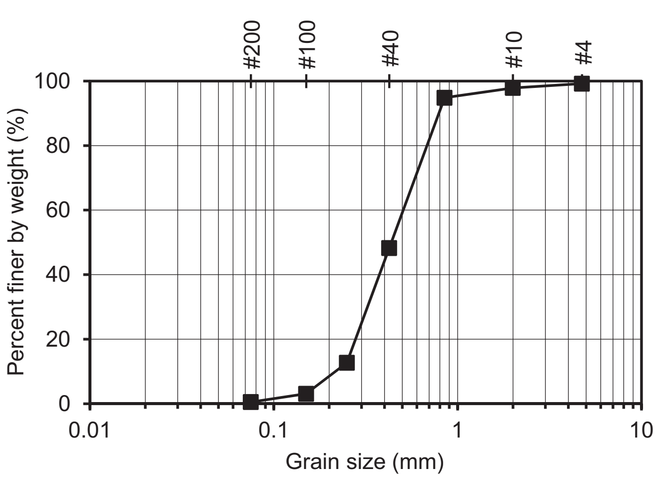

Fig. 9. Particle size distribution of soil specimen.

average internal friction angle verified by the direct shear tests is 31.63° and the average cohesion is 16.7 kPa, as shown in Table 3 (Kim, 2008).

There were some minor differences between the results from direct shear tests and the newly developed strip loading testing device and method. The slight difference could easily be appreciated as the developed strip loading test simulates real-world strip footing failure mechanism using a relatively large soil specimen (12.5 in × 10 in × 6 in or 317 mm × 254 mm × 152 mm) as shown in the sand box which can be simplified as a plane strain problem, while in the direct shear tests, small sandy soil specimen with dimensions of approximately 50.8 mm (2 in) in diameter and 25.4 mm (1 in) in height is used. The second reason could be due to the fact that the soil specimens were not exactly of the same state of density. Thirdly, the loading rate of direct shear test was more precise and consistently controlled while the strip loading test was initially manually controlled. The preliminary initial internal friction angles estimated by the new method seems to be smaller than the results obtained from direct shear tests, but the measured cohesions are generally lower than those obtained from direct shear tests. The discrepancy could also be explained partly due to the sandy granular material overflow outside the failure plane on the horizontal surface which perhaps makes estimation of deformation range R_d be overestimated. Herein, the overflow soils are still within the sandbox and none of the soil mass is lost. But the overflow soil may cover the actual shear band deformation range R_d. The ranges of calculated cohesion values obtained from strip loading tests appear to agree well compared with the results obtained from the direct shear test. On average, however, the estimated cohesions from strip loading tests are smaller, on the conservative sides, than those obtained from direct shear test.

Based on Li (2005), Kim (2008) further refined the developed strip loading test method by performed additional six groups of strip loading tests on mixed soil, as shown in Table 3. It can be seen that the accuracy of strip loading test results was improved. This may partly due to the testing procedure refinement and interpretation consideration of the soil overflow and/or shear band phenomenon as reported in Kim (2008).

Plotting the comparison results obtained from the developed strip loading tests and direct shear tests within Fig. 12 shows the general trend of measured soil strength parameters estimated. It can be seen from Fig. 12 that during the first initial stage of strip loading test, the internal friction angle measured has relatively larger values than those reported by Kim (2008) whose data are more precisely focused and the bias between direct shear and strip loading tests are more close to 1. This could have been due to the fact that the strip loading test equipment has been better calibrated, additional shear band formation is considered to help better

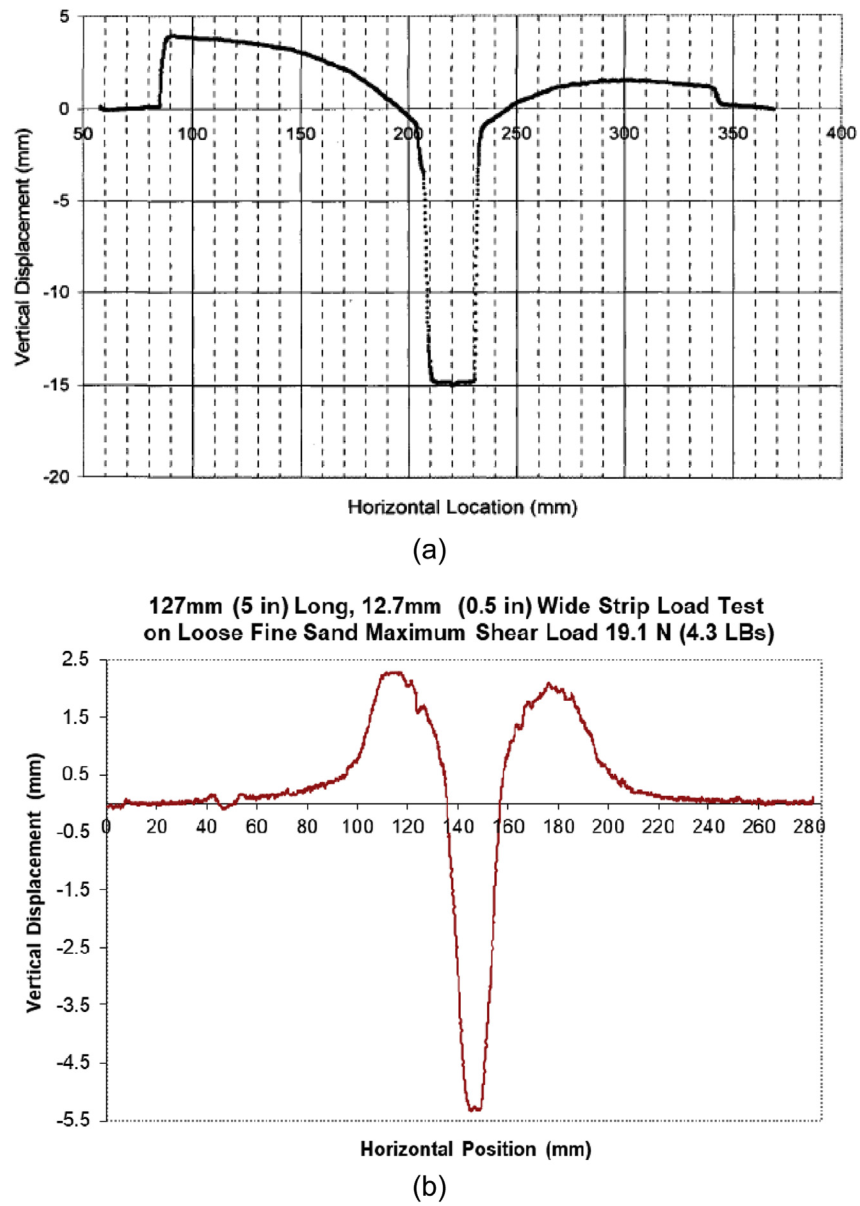

Fig. 10. Deformation profile scanned with OTDM: (a) Kim (2008), and (b) This study.

estimate the deformation range R_d, and thus more precise and narrow ranges of both cohesion and internal friction angle are measured which are more closely to those results obtained from direct shear tests. Fig. 12 also shows that the cohesion estimated by Li (2005) is close to those obtained from direct shear test and from Kim (2008). Generally, the soil cohesion measured from strip loading tests tends to be on the conservative sides, as the bias of the ratio between direct shear test values over strip loading test values is above the 1:1 slope trend, as seen in Kim (2008). This first initially developed strip loading test methods by Li (2005) may overestimate the soil internal friction angle while Kim (2008) may underestimate the soil strength parameters, but it will generally lead to a more conservative and safe design compared with the case using the strength parameters obtained from direct shear tests.

This newly developed strip loading tests and modeling device had been used to demonstrate the concept of soil strength properties with a success in the author's different geotechnical and materials science and basic mechanics courses instructions including soil mechanics, soil engineering and a basic mechanics I – statics course as well. The newly proposed and developed strip loading test method can give students in geotechnical engineering and foundation engineering an intuitive and visually clear understanding of how the soil strength properties affect the soil surface deformation and failure loads. This developed strip loading test also helps to connect entry-level elementary engineering design, engineering mechanics course with upper-level major and senior design courses instructions. Further modifications, revisions and improvement could also help with the research study of sandy soils liquefaction effects, bio-modified soils research study as well as regolith properties estimation.

7. Concluding remarks

A new experimental method of soil characterization based on the surface displacement of strip loaded soils is developed which uses a novel, non-contact distance measurement technique. The theoretical foundations of strip loading test were based on the theoretical equations Eqs. (14)–(16) derived and reported by Li

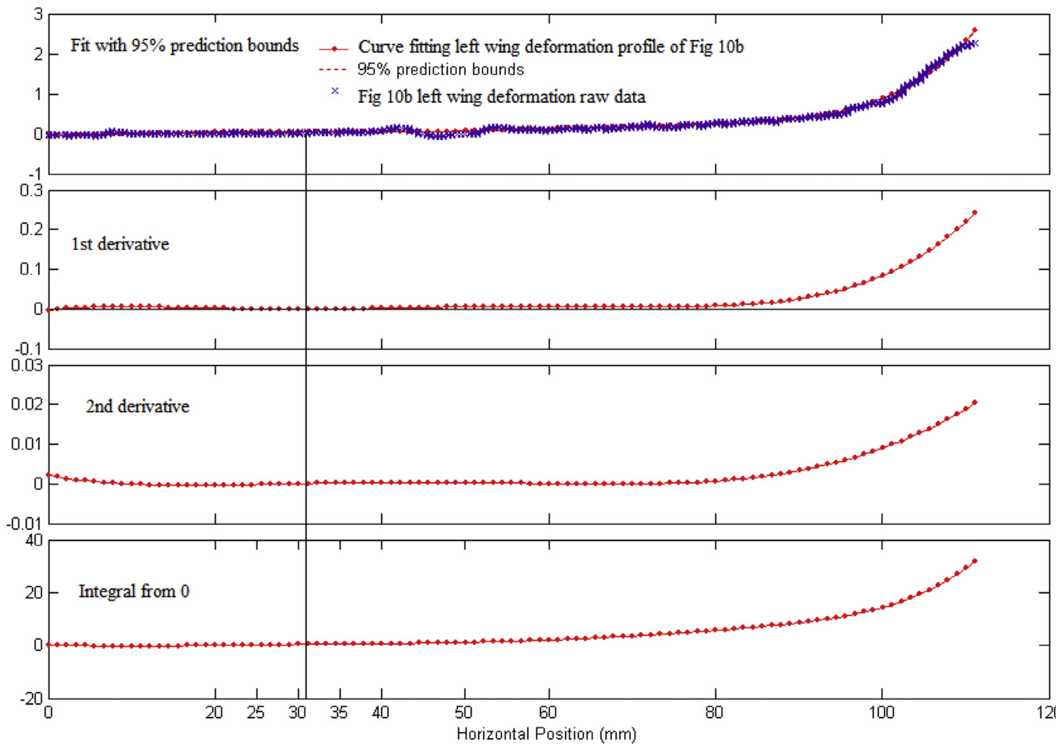

Fig. 11. Left wing of deformation profile of Fig. 10b to estimate deformation range R_d.

Table 1
Soil strength parameters interpreted from strip loading test results.

Source	Soil type	Width (mm) × Length (mm), D_r (%)	Average R_d (mm)	ϕ (°)	c (kPa)
Li (2005)	Loose sandy soil specimens prepared without compaction	12.7 × 127	103	40.1	1.179
		12.7 × 127	106	41.2	2.378
		12.7 × 127	124	42.6	3.916
		Average	111	41.3	2.491
		19.05 × 127	134	38.1	1.482
		19.05 × 127	132	37.9	3.792
		Average	133	38	2.637
Kim (2008)	Sand, silt and clay mixed soil specimens	19.05 × 127, Specimen group 1, D_r = 83	88.48	34.69	1.225
		19.05 × 127, Specimen group 2, D_r = 78	61.98	28.68	4.41
		19.05 × 127, Specimen group 3, D_r = 76	75.48	32.15	2.95
		Average	75.31	31.84	2.862
		25.4 × 127, Specimen group 2, D_r = 78	102.8	32.66	4.16
		25.4 × 127, Specimen group 3, D_r = 76	87.3	29.87	5.67
		25.4 × 127, Specimen group 4	116.8	34.995	13.76
		Average	102.3	32.51	7.862

Note: D_r denotes the relative density of the soil specimens.

Table 2
Verification of soil strength parameters for loose sandy soil specimens interpreted from direct shear test results (after Li, 2005).

Test No.	ϕ (°)	c (kPa)
1	36.1	9
2	30	25
3	33.8	9
4	36.9	6
5	33	0
6	36.9	7
7	37.3	0
8	36.7	0
9	36.9	7
10	35.3	7
Average of all	35.3	7
Average (except #2)	36	7

(2005) and then further refined by Kim (2008) by considering the shear band effects on the surface deformation range calibration. The originally developed Eq. (16) by Li (2005) appears to be the generalized testing applicable to the special zero confining pressure triaxial shear test, and unconfined compression test of clay with a close to zero degree of internal friction angle. The surface deformation range (Eq. (15)) is applicable for example to the special cases of fully saturated clay soil wherein the deformation range is reduced to full strip width, $2X$, by considering a full circle limit equilibrium (Budhu, 2011). Also, the generalized cohesion equation (Eq. (16)) can be reduced to the form of $c = 0.5q_u$ for unconfined compression test and hand-held pocket penetration test. Thus, the unconfined compression test can be considered as a special case of the developed strip loading test based on the analysis of derived equations.

Table 3
Verification of soil strength parameters for mixed soil specimens interpreted from direct shear test results (after Kim, 2008).

Soil specimen	Mean particle size, d_{50} (mm)	Ultimate bearing capacity, q_u (kPa)	Internal friction angle, ϕ (°)			Cohesion, c (kPa)		
			Direct shear test	New strip loading test method		Direct shear test	New strip loading test method	
				Terzaghi model	Vesic model		Terzaghi model	Vesic model
Group 1	0.333	50.75	32.23	31.94	32.44	11.71	1.43	1.37
Group 2	0.295	126.71	32.56	32.07	32.46	17.33	3.52	3.41
Group 3	0.29	123.18	30.11	29.9	30.31	21.07	4.17	4.03
Average			31.63	31.3	31.67	16.7	3.04	2.94

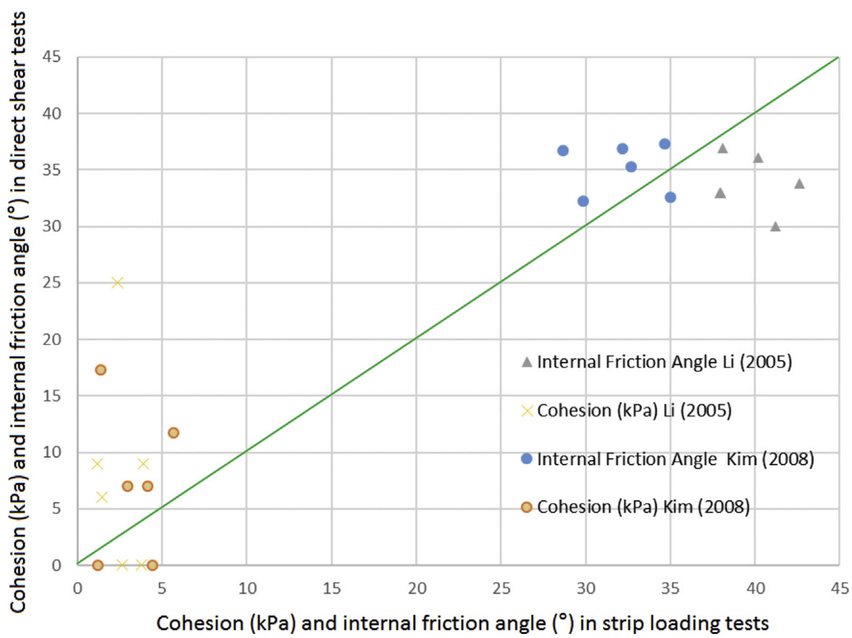

Fig. 12. Comparison between strip loading test and direct shear test results. Both cohesion and internal friction angle are plotted in the same figure for comparison.

The average internal friction angle derived from the newly developed testing method, for the strip with the width of 12.7 mm (0.5 in), matches reasonably well with that derived from direct shear testing. This new strip loading testing method provides a quick approximate method for estimating the soil strength properties.

Compared with the traditional direct shear test and the triaxial shear test, the new testing method is relatively easier to perform. It also simulates the actual failure more visually realistic as often occurs in the real world. Unlike the direct shear test and the triaxial shear test, the new testing concept could be further applied for in situ tests to modeling both drained and undrained soil strength properties. The developed new strip loading test provides a plane strain modeling test device and method which could be used for benchmarking verification test for many existing and newly proposed constitutive modeling devices. For example, the bulging boundary provides sufficient data for deep learning neural network based constitutive modeling training (Li et al., 2000). Further refinement of the strip loading test may also be used for earthquake-related fault activation shear band formation studies. It may also be utilized for testing bio-modified soil specimen testing. Transparent soils could also be utilized in further study for either engineering educational research or geotechnical investigations of soil strength and bearing capacity. Updated and similarly improved version of the strip loading test might also be installed on a planetary rover for wheels' loading test for quickly estimating the soil properties on Earth extra-terrestrial planet, like Mars' surface regolith materials explorations.

The newly developed strip loading test method provides an intuitive understanding of strip footing general shear failures and soil strength properties such as cohesion c and internal friction angle ϕ by measuring surface deformation range and failure load. As the induced stress along the slip surface could be different at different locations, theoretically there is a friction angle for each point along the slip surface or shear band. In the proposed new strip loading tests, a single friction angle is estimated based on the general bearing capacity failure mechanism. It is worthy to make a note that the evaluated soil shear strength parameters are not necessarily the peak values at a certain fixed point, but rather representative soil strength parameters representative of the entire slip mechanism that forms beneath the strip footing. The estimated soil strength parameters therefore account for the contribution from every element along the slip surface.

The developed strip loading test results on the same soils indicate that it can provide a relatively conservative and safe design compared with the strength parameters measured from direct shear test results. The developed soil strip loading test device can also be used as an effective teaching tool for learning bearing capacity concept.

Conflicts of interest

The author wishes to confirm that there are no known conflicts of interests associated with this publication and there has been no significant financial support for this work that could have influenced its outcome.

Acknowledgements

The author is grateful to the anonymous reviewers and experts' discussion feedback for their helpful constructive comments and suggestions. Their expert opinions helped to improve the paper over the years. The author's advisers and mentors are also sincerely thanked for their invaluable suggestions, mentoring guidance and advice. Teaching and research assistantship funding supports during his study and work at University of Alabama and University of Akron were acknowledged. The research accommodation and encouraging support at all the institutions and organizations involved are sincerely appreciated. Students in the author's current university undergraduate statics, elementary engineering design, materials sciences and geotechnical engineering classes are all gratefully appreciated for providing an educational survey feedback on the effectiveness of the developed strip loading test device as a teaching aid.

References

Beer FP, Johnston ER, Mazurek DF. Statics, vector mechanics for engineers. 12th edition. McGraw Hill; 2019.
Bishop AW, Henkel DJ. Test measurement of soil properties in the triaxial test. London: Arnold; 1962.
Bishop AW, Wesley LD. A hydraulic triaxial apparatus for controlled stress path testing. Géotechnique 1975;25(4):667–70.
Bolton MD. The strength and dilatancy of sands. Géotechnique 1986;36(1):65–78.
Bucher GM. Demonstration models for undergraduate teaching geotechnics. In: Proceedings of the 1st International Conference on geotechnical engineering education and training. Rotterdam, The Netherlands: A.A. Balkema; 1986. p. 325–8.
Budhu M. Soil mechanics and foundations. 3rd ed. John Wiley and Sons, Inc.; 2011.
Chen WF, Baladi GY. Soil plasticity: theory and implementation. Elsevier; 1985.
Chen ZY, Zhou JX. Soil mechanics. Tsinghua University Press; 2008.
Coulomb CA. Essai sur une application des règles de maximis et minimis à quelques problèmes de statique realtifs à l'architecture. In: Mémoires de meathÉmatique et de Physique préSenté à l'Académie Royale des Science; 1776. p. 343–82 [in French].
Cui YJ, Sultan N, Delage P. A thermomechanical model for clays. Canadian Geotechnical Journal 2000;37(3):607–20.
Darwin GH. On the horizontal thrust of a mass of sands. Minutes of the Proceedings of the Institution of Civil Engineers 1883;71:350–78.
Das BM. Theoretical foundation engineering. Elsevier; 1987.
Das BM. Advanced soil mechanics. 3rd ed. Taylor & Francis; 2008.
Das BM. Principles of foundation engineering. 8th ed. Cengage Learning; 2016.
Das BM. Principles of geotechnical engineering. 9th ed. Cengage Learning; 2018.
De Beer EE, Vesic A. Etude experimentale d la capacite portante du sable sous des fondations directes establies en surface. Annales des Travaux Publics de Belqique 1958;59(3):5–58 (in French, De Beer EE, Vesic A., Experimental study of the carrying capacity of sand under direct foundations established on the surface. Annals of Public Works of Belgium 1958).
Ferguson ES. Engineering and the mind's eye. MIT Press; 1992.
Gadry F. Mémorie sur la Poussée des Terres. Summarized by Mayniel in 1808. 1746 [in French].
Guo P, Philips R, Popescu R. In: Proceedings of the physical modelling in Geotechnics. St. Johns; 2002.
Hibbeler RC. Engineering mechaniCcs – statics. 14th ed. Pearson; 2016.
Holtz RD, Kovacs WD, Sheahan TC. An introduction to geotechnical engineering. 2nd edition. Prentice Hall; 2011.
Jefferies MG. Nor-Sand: a simple critical state model for sand. Géotechnique 1993;43(1):91–103.
Kim J. Development of new soil testing method to determine shear strength parameters of soil. PhD Thesis. Department of Civil, Construction and Environmental Engineering, The University of Alabama at Tuscaloosa; 2008.
Leshchinsky D, Marcozzi GF. Bearing capacity of shallow foundations: rigid versus flexible models. Journal of Geotechnical Engineering 1990;116(11). https://doi.org/10.1061/(ASCE)0733-9410(1990)116:11(1750).
Li J, Gao Q, Ren T, Zhu J. Engineering materials constitutive modeling and its parameters' back analysis. Journal of Hebei Polytechnic University: Natural Science Edition 2000;22(4):1–11.
Li J. Geomaterial characterization with displacement measurement technique and finite element simulation. PhD Thesis. Department of Civil, Construction and Environmental Engineering, The University of Alabama at Tuscaloosa; 2005.
Li J, Zhai J. Subsidence modeling and analysis for sand shear strength parameter testing. In: Proceedings of the SEM (society of experimental mechanics) annual Conference and exposition on experimental and applied mechanics; 2015.
Li J, Park D, Barkey ME. Soil strength characterization by strip loading technique. In: Proceedings of the 60th Canadian geotechnical Conference and 8th joint CGS/IAH-CNC groundwater Conference; 2007. p. 1733–66.
Mohr O. Welche Umstände Bedingen die Elastizitätsgrenze und den Bruch eines Materials? Zeitschrift des Vereines Deutscher Ingenieure 1900;44:1524–30 (in German).
Park DW, Li J. Subsidence simulation using laser optical triangulation distance measurement devices. In: Gulf rocks 2004, the 6th North America rock mechanics symposium (NARMS): rock mechanics across borders and disciplines; 2004.
Prandtl L. Uber die Eindringungs-festigkeit (Harte) plastischer Baustoffe und die Festigkeit von Schneiden. Zeitschrift fur Angewandte Mathematik und Mechanik 1921;1:15–20 (in German).
Rowe PW. The stress-dilatancy relation for static equilibrium of an assembly of particles in contact. Proceedings of the Royal Society A 1962;269(1339):500–27.
Scott RF. Principles of soil mechanics. Addison-Wesley Publishing Company, Inc.; 1963.
Taylor DW. Fundamentals of soil mechanics. John Wiley and Sons, Inc.; 1948.
Terzaghi K. Theoretical soil mechanics. John Wiley and Sons, Inc.; 1943.
Terzaghi K, Peck RB, Mesri G. Soil mechanics in engineering practice. John Wiley and Sons, Inc.; 1996.
Vesic AS. Analysis of ultimate loads of shallow foundations. Journal of the Soil Mechanics and Foundations Division 1973;99(1):45–73.
Wartman J. Geotechnical physical modeling for education: learning theory approach. Journal of Professional Issues in Engineering Education and Practice 2006;132(4). https://doi.org/10.1061/(ASCE)1052-3928(2006)132:4(288).
Whittle AJ. MIT-E3: a constitutive model for over consolidated clays. In: Computer methods and advances in geomechanics. A.A. Balkema; 1991.
Wood DM. Geotechnical modeling. CRC Press; 2004.
Zhang F, Ikariya T. A new model for unsaturated soil using skeleton stress and degree of saturation as state variables. Soils and Foundations 2011;51(1):67–81.

Dr. Jiliang Li is working as an Assistant Professor of Civil Engineering at Purdue University Northwest. He has industrial work experience in several states with projects consulting experience ranging from residential, commercial and subdivision projects to larger scale state DOT (Department of Transportation) and federal projects. Dr. Li has teaching and research interests ranging from engineering education, engineering mechanics encompassing statics, soil dynamics, mechanics of materials and geotechnics (geomechanics, rock mechanics, soil mechanics, engineering geology and surface water hydrology), probability and statistics applications in civil engineering, reliability based load and resistance factor design (LRFD) of geotechnical structures, design of earth structures, soil and rock exploration, geotechnical and foundation engineering in particular.